Analysis of *Drosophila* Segmentation Network Identifies a JNK Pathway Factor Overexpressed in Kidney Cancer

Jiang Liu[1,2,*], **Murad Ghanim**[1,2,*,†], **Lei Xue**[3,*], **Christopher D. Brown**[1,2], **Ivan Iossifov**[1,4,‡], **Cesar Angeletti**[5], **Sujun Hua**[1,2], **Nicolas Nègre**[1,2], **Michael Ludwig**[1,2,6], **Thomas Stricker**[1,2,7], **Hikmat A. Al-Ahmadie**[7], **Maria Tretiakova**[7], **Robert L. Camp**[5], **Montse Perera-Alberto**[8], **David L. Rimm**[5], **Tian Xu**[3], **Andrey Rzhetsky**[1,4], and **Kevin P. White**[1,2,6,§]

[1] Institute for Genomics and Systems Biology, The University of Chicago and Argonne National Laboratory, Chicago, IL, USA

[2] Department of Human Genetics, The University of Chicago, Chicago, IL, USA

[3] Howard Hughes Medical Institute, Department of Genetics, Yale University School of Medicine, New Haven, CT, USA

[4] Department of Medicine, The University of Chicago, Chicago, IL, USA

[5] Department of Pathology, Yale University School of Medicine, New Haven, CT, USA

[6] Department of Ecology and Evolution, The University of Chicago, Chicago, IL, USA

[7] Department of Pathology, The University of Chicago, Chicago, IL, USA

[8] Department of Anatomy, La Laguna University, La Laguna, Tenerife, Spain

Abstract

We constructed a large-scale functional network model in *Drosophila melanogaster* built around two key transcription factors involved in the process of embryonic segmentation. Analysis of the model allowed the identification of a new role for the ubiquitin E3 ligase complex factor SPOP. In *Drosophila,* the gene encoding SPOP is a target of segmentation transcription factors. *Drosophila* SPOP mediates degradation of the Jun-kinase phosphatase Puckered thereby inducing TNF/Eiger dependent apoptosis. In humans we found that SPOP plays a conserved role in TNF-mediated JNK signaling and was highly expressed in 99% of clear cell renal cell carcinoma (RCC), the most prevalent form of kidney cancer. SPOP expression distinguished histological subtypes of RCC and facilitated identification of clear cell RCC as the primary tumor for metastatic lesions.

Over the last three decades, extensive molecular and genetic analyses have characterized the identity of and interactions between components of the *Drosophila* segmentation process (1). Maternal factors distributed in gradients along the anterior-posterior (A-P) axis activate zygotic transcription of gap genes, which encode transcription factors that activate sets of pair-rule genes including the homeobox transcription factors Even-skipped (Eve) and Fushi tarazu (Ftz). These pair rule proteins then directly regulate segment polarity genes that determine the internal A-P orientation of each segment. Many of the human homologs of these genes and their down-stream targets play critical roles in human diseases, especially cancers (2,3). In an effort to extract new information from the *Drosophila* segmentation network, as well as to mine this

§To whom correspondence should be addressed. E-mail: kpwhite@uchicago.edu.
*These authors contributed equally to this work.
†Present address: Department of Entomology, The Volcani Center, Bet Dagan, Israel.
‡Present address: Cold Spring Harbor Laboratory, One Bungtown Road, P.O. Box 100, Cold Spring Harbor, NY 11742, USA.

network for novel disease related genes, we built a large-scale predictive network model around Ftz and Eve.

We analyzed gene expression changes between individual wild type embryos and embryos with null mutations in *ftz* and eve (4,5) collected during a developmental time course from 2 hr until 7 hr after egg laying (AEL). By focusing on Ftz and Eve effects 2 to 3 hours AEL (early zygotic expression), we found 1310 genes differentially expressed between the *ftz* mutant and wild type, and 1074 genes differentially expressed between the *eve* mutant and wild type (false discovery rate < 0.001, table S1, S2).

Using antibodies specific for Ftz or Eve, we performed chromatin immunoprecipitation (ChIP) and mapped genome-wide transcription factor binding in cellular blastoderm embryos 2 hours AEL on custom designed high density DNA microarrays (4). We found 1286 Ftz and 1499 Eve bound probes (intensity P < 0.0001 and Z score > 1.96, see supplemental method; 21 probes on both lists map within 500bp). We analyzed several methods for probe to target gene mapping to maximize the overlap between the differentially expressed and ChIP target gene sets (see supplemental methods; fig. S1). The greatest such enrichment was obtained by designating genes within 1kb of a binding site as targets. At this threshold, we identified 969 Ftz ChIP-chip target genes and 932 Eve ChIP-chip target genes (overlap 175 genes; table S3, S4).

Genes both differentially expressed and targeted by ChIP-chip binding site mapping were considered as putative direct target genes. We thus identified 137 Ftz direct target genes (Fig. 1A) and 98 Eve direct target genes (fig. S2; overlap 9 genes). Fig. 1A (right panel) shows the locations of binding sites at Ftz or Eve direct target genes. Analysis of direct target gene annotations indicates 39 genes (21%) regulate transcription and 74 genes (40%) are involved in developmental processes (Fig. 1A, center panel); both annotation classes were significantly enriched compared to the 9.6% and 18% of *Drosophila* genes annotated as transcriptional or developmental regulators, respectively (p=1.05×10^{-6} and p=1.81×10^{-12}; hypergeometric test). A complete target list can be found in tables S5 and S6.

To extend our Ftz-Eve network model beyond direct transcriptional regulation, we included automated literature mining methods to capture published interactions of target genes (5). We then integrated yeast two-hybrid based protein-protein interaction data (6) into our model by connecting protein interactions between existing components in the network. To limit the size of the network, we extended the protein-protein interaction only one degree from the direct targets of Ftz or Eve. The resulting Ftz-Eve regulatory network model included 4084 genes/proteins and 6648 interactions between them (fig. S3).

To confirm parts of the network model topology we examined several genes that are expressed in segmental patterns (7) and validated a limited set of interactions by genetic and biochemical testing of simple predictions from our network model (fig. S4),

Analysis of the Eve-Ftz network identified 150 different genes as direct targets of Eve or Ftz that also have unambiguous human homologs. From this gene set, we identified a top candidate, *CG9924* or *roadkill (rdx)*, which ranks first in network betweenness-centrality and thus constitutes a major network hub (8) (see supplemental methods, table S8). The *rdx* gene encodes a BTB domain protein that has been recently shown to act to regulate Cubitus interruptus (Ci) degradation in the Hedgehog pathway (9,10). This product of the *rdx* gene is 79% identical to the human protein SPOP and these proteins appear to be orthologs (fig. S5) (9,10); we refer to the *rdx* gene product(s) as *Drosophila* SPOP (D-SPOP).

Our network model indicates that the *D-SPOP* gene is a direct target of Ftz at 2–3 hours AEL and that the D-SPOP protein interacts with the Jun Kinase phosphatase Puckered (Puc) (Fig. 1B). RNA *in situ* hybridizations for *D-SPOP mRNA* in *ftz* mutant embryos confirmed that *ftz*

is indeed required for *D-SPOP* expression in parasegments that normally express Ftz (Fig. 1C). We did not observe significant mis-expression of *D-SPOP* mRNA in *eve* mutant embryos at 2–3 hours AEL (fig. S6), suggesting that the Ftz effects on *D-SPOP* mRNA levels occurs in advance of the Eve effect. We found that the D-SPOP protein segmental expression pattern was completely lost in *eve* mutant embryos 6–7 hours AEL (Fig. 1D), behaving similarly to the well-characterized Ftz and Eve target gene *engrailed* (11,12). Previous studies also indicate that D-SPOP is regulated by Hedgehog (Hh) later in development, indicating another layer of D-SPOP regulation by the segment polarity system (9). Together, these data strongly indicate that *D-SPOP* expression is downstream of the pair-rule genes in the segmentation hierarchy.

RNAi knockdown of *D-SPOP* mRNA levels and P-element insertion mutagenesis of the *D-SPOP* gene resulted in severe and consistent disruption of both the peripheral and the central nervous system (CNS) (fig. S7). Such phenotypes are recapitulated by mutating *ftz* or *eve* and are likely due to mid-embryonic functions of D-SPOP when Ftz and Eve become active in the CNS (13,14). Furthermore, it was recently demonstrated that the *Drosophila* Eiger/TNF pathway regulates embryonic neuroblast division (15). Thus we hypothesized that the function of D-SPOP in nervous tissue development may result from its interaction with Puc, which mediates a feedback loop by negatively regulating *basket* (*Drosophila* JNK) in the *Drosophila* Eiger/Tumor Necrosis Factor (TNF) pathway (16) (Fig. 1B).

In *Drosophila*, ectopic expression of Eiger in neuronal cells in the developing eye induces apoptosis through the JNK pathway, resulting in a reduced adult eye size (Fig. 2A, 2B) (17). Deletion of one wild-type copy of *D-SPOP* or RNAi knock down of *D-SPOP* mRNA partially suppresses the eye phenotype of Eiger expression (Fig. 2C, 2D). Additionally, ectopic expression of D-SPOP in the developing eyes produces a small and rough eye phenotype (Fig. 2E). Analysis of genetic interactions between the genes encoding D-SPOP and other members of the Eiger-JNK pathway (fig. S8), indicates that D-SPOP is acting downstream of dTAK1 (JNKKK) and Hep (JNKK) and upstream of Bsk (JNK) and Puc. Our experiments therefore indicate that D-SPOP functions as an essential positive regulator for Eiger triggered apoptosis, consistent with the interaction between D-SPOP and Puc predicted in the Ftz-Eve network model.

A physical interaction between D-SPOP and Puc was confirmed by both *in vitro* pulldown and *in vivo* immunoprecipitation assays (Fig. 2F, 2G). D-SPOP contains two conserved domains, a MATH domain and a BTB/POZ domain (18). MEL-26, the *Caenorhabditis elegans* ortholog of human SPOP, was first identified as a BTB protein that serves as an adaptor of Cul3 based ubiquitin ligase (18). Recently, human SPOP has been shown to mediate ubiquitination of death domain-associated protein (Daxx) (19), the Polycomb group protein BMI-1, the histone variant MacroH2A (20), and the transcription factor Gli (10). We found that Puc protein levels were significantly reduced when co-expressed with D-SPOP in S2 cells (Fig. 2H). Furthermore, D-SPOP promoted Puc ubiquitination in S2 cells treated with the proteasome inhibitor MG132 (Fig. 2I). Taken together, these results indicate that D-SPOP induces apoptosis in the Eiger/TNF pathway by the mediating Puc ubiquitination and degradation (Fig. 2J).

Homologs of several Ftz and Eve targets have been shown to be involved in human cancers (21), a large body of experimental and clinical data indicates that defects in ubiquitin signaling pathways have roles in the genesis of different tumor types (22), and JNK activation is required for cellular transformation induced by RAS, an oncogene mutated in 30% of human cancers (23). To determine whether human SPOP's role in modulating TNF stimulated JNK signaling is conserved, we treated HEK293 cells over-expressing SPOP with TNF-α, then analyzed phosphorylated JNK (P-JNK) and phosphorylated c-Jun (P-c-Jun) levels. Consistent with its role in *Drosophila* as an activator of the pathway, overexpression of SPOP increases the level

of P-JNK and P-c-Jun, indicating conservation of its function in modulating the JNK pathway (Fig. 3A).

To test whether SPOP is associated with human cancers, SPOP protein expression levels were screened with tissue microarrays that contained 20 tumors from each of 18 different organs. We found that 85% of renal cell carcinomas (RCC) showed high expression of SPOP, while normal kidney tissue was uniformly negative (Fig 3B; Table 1). To further investigate the potential of SPOP as a marker, we designed a large tissue array containing more than 300 RCC samples. 77% of the tumor samples were positive for SPOP staining; normal kidney samples were all negative (Table 2).

RCC is a heterogeneous group of tumors with distinct histological subtypes, including clear cell, papillary, chromophobe and other rare subtypes in addition to oncocytoma, which is a benign solid renal tumor (24). The majority of RCC is of clear cell type, comprising up to 75%. While the majority of RCCs can be subtyped by hematoxylin + eosin staining morphology, diagnostic difficulties arise when clear cell RCCs display morphologic features that overlap with other RCC subtypes and non-renal tumors (25–27). Currently, a panel of immunohistochemical markers is used to differentiate the major subtypes of RCC in difficult cases (26,27). Unfortunately, these panels lack a specific and sensitive marker that is positive in clear cell RCC (26,27). Recently Carbonic Anhydrase IX has been proposed as a positive marker for clear cell RCC, but it is positive in other RCCs and several other tumor types as well (28–30). Patient tumor samples in our studies were classified into different types according to the recent World Health Organization (WHO) classification system. We found that 99% of the clear cell RCC and 86% of the chromophobe RCC showed positive staining for SPOP, but only 22% of papillary-type RCC were SPOP positive. Four out of 31 papillary RCCs from the general pathology reports were shown to be misdiagnosed as clear cell RCCs when the tumor biopsies were re-analyzed by urological pathologists. All four of these misdiagnosed RCCs have papillary architecture and were subsequently shown to stain positive for SPOP. Our tissue array also included benign oncocytomas, which can mimic renal cell carcinoma both clinically and pathologically, in turn potentially subjecting patients to unnecessary surgeries and additional morbidities. Only 6% of oncocytomas showed weak positive staining. These results indicate that SPOP is a highly sensitive and specific diagnostic biomarker for clear cell RCC and can help distinguish histological subtypes of RCC.

Up to 30% of RCC patients present with metastases; half of the rest will develop metastases later in their course, 90% of which are clear cell RCCs. Accordingly, we further screened for SPOP staining in confirmed metastases from RCC and found that 97% of them were positive (Table 3), indicating that SPOP may be a useful biomarker to identify clear cell RCC as the site of the primary tumors in cases of metastases from unknown origin. Taken together, our results demonstrate that novel functions for conserved molecules can readily be extracted from data mining of large scale networks in *Drosophila*, and provide a strategy for rapid identification of factors that may have clinical relevance as biomarkers or drug targets for human diseases.

Supplementary Material

Refer to Web version on PubMed Central for supplementary material.

References and Notes

1. Nasiadka, A.; Dietrich, BH.; Krause, HM. Anterior-Posterior Patterning in the Drosophila Embryo. In: DePamphilis, M., editor. Advances in Developmental Biology and Biochemistry. Vol. 12. Elsevier Science B.V; 2002. p. 155

2. Hahn SA, et al. Science Jan 19;1996 271:350. [PubMed: 8553070]

3. Johnson RL, et al. Science Jun 14;1996 272:1668. [PubMed: 8658145]

4. Stolc V, et al. Science Oct 22;2004 306:655. [PubMed: 15499012]

5. Rzhetsky A, et al. J Biomed Inform Feb;2004 37:43. [PubMed: 15016385]

6. Giot L, et al. Science Dec 5;2003 302:1727. [PubMed: 14605208]

7. Tomancak P, et al. Genome Biol 2007;8:R145. [PubMed: 17645804]

8. Jeong H, Mason SP, Barabasi AL, Oltvai ZN. Nature May 3;2001 411:41. [PubMed: 11333967]

9. Kent D, Bush EW, Hooper JE. Development May;2006 133:2001. [PubMed: 16651542]

10. Zhang Q, et al. Dev Cell Jun;2006 10:719. [PubMed: 16740475]

11. Harding K, Rushlow C, Doyle HJ, Hoey T, Levine M. Science Aug 29;1986 233:953. [PubMed: 3755551]

12. Jaynes JB, Fujioka M. Dev Biol May 15;2004 269:609. [PubMed: 15110723]

13. Doe CQ, Hiromi Y, Gehring WJ, Goodman CS. Science Jan 8;1988 239:170. [PubMed: 2892267]

14. Broadus J, et al. Mech Dev Nov;1995 53:393. [PubMed: 8645605]

15. Wang H, Cai Y, Chia W, Yang X. Embo J Dec 13;2006 25:5783. [PubMed: 17139248]

16. Martin-Blanco E, et al. Genes Dev Feb 15;1998 12:557. [PubMed: 9472024]

17. Igaki T, et al. Embo J Jun 17;2002 21:3009. [PubMed: 12065414]

18. Xu L, et al. Nature Sep 18;2003 425:316. [PubMed: 13679922]

19. Kwon JE, et al. J Biol Chem May 5;2006 281:12664. [PubMed: 16524876]

20. Hernandez-Munoz I, et al. Proc Natl Acad Sci U S A May 24;2005 102:7635. [PubMed: 15897469]

21. Potter CJ, Turenchalk GS, Xu T. Trends Genet Jan;2000 16:33. [PubMed: 10637629]

22. Hoeller D, Hecker CM, Dikic I. Nat Rev Cancer Oct;2006 6:776. [PubMed: 16990855]

23. Weiss C, Bohmann D. Cell Cycle Feb;2004 3:111. [PubMed: 14712066]

24. Cohen HT, McGovern FJ. N Engl J Med Dec 8;2005 353:2477. [PubMed: 16339096]

25. Rosai, J. Rosai and Ackerman's Surgical Pathology. Mosby; New York: 2004.

26. Skinnider BF, Amin MB. Semin Diagn Pathol Feb;2005 22:51. [PubMed: 16512599]

27. Zhou M, Roma A, Magi-Galluzzi C. Clin Lab Med Jun;2005 25:247. [PubMed: 15848735]

28. Al-Ahmadie HA, et al. Am J Surg Pathol Mar;2008 32:377. [PubMed: 18300814]

29. Leibovich BC, et al. J Clin Oncol Oct 20;2007 25:4757. [PubMed: 17947723]

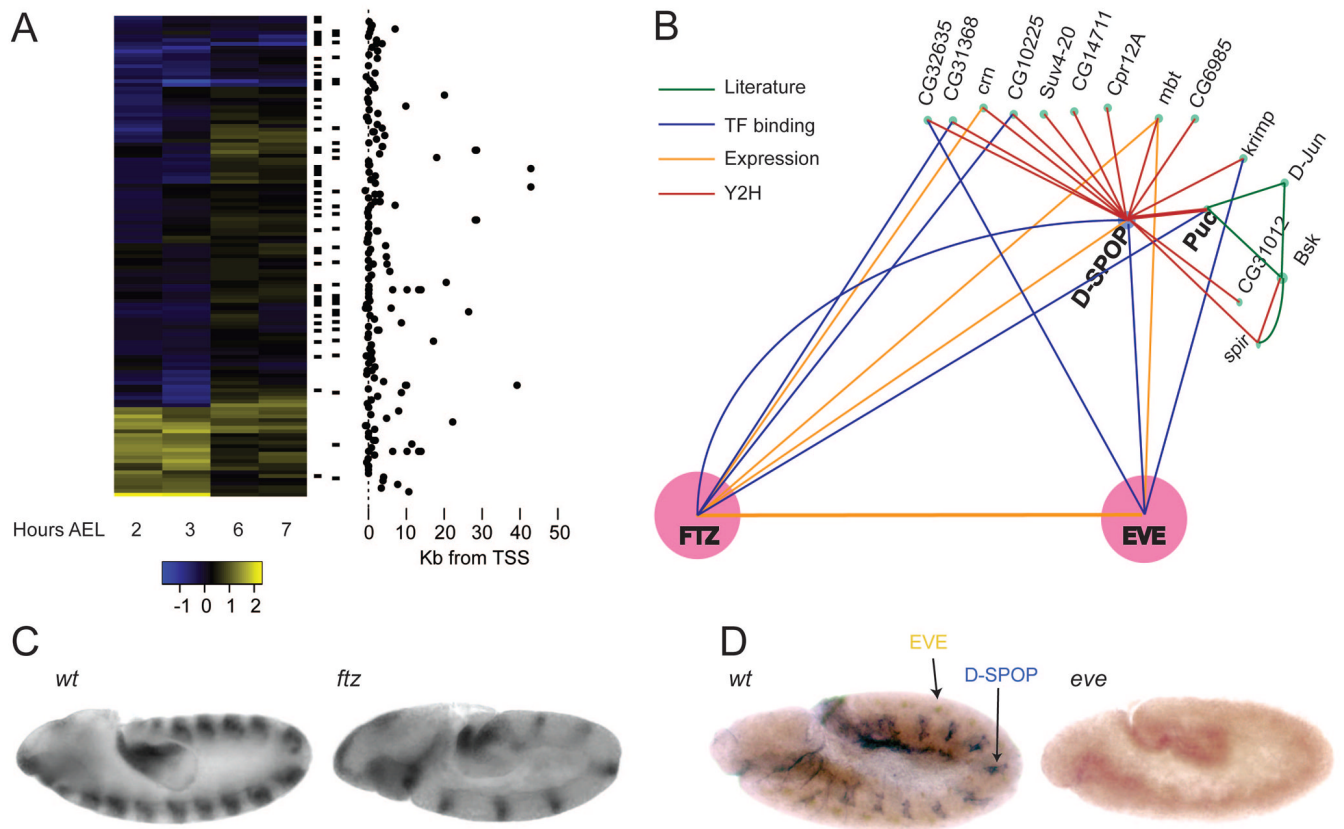30. Potter C, Harris AL. Cell Cycle Feb;2004 3:164. [PubMed: 14712082]

Fig. 1.

Drosophila segmentation network. (**A**) Identification of direct targets of Ftz. Heatmap at left depicts $\log_2$-fold change in gene expression, mutant vs. wild type. Columns represent time points in hours after egg laying (AEL). Rows depict individual genes, sorted by hierarchical clustering. Genes involved in regulation of development (left tick marks) or transcriptional regulation (right tick marks) from gene ontology (GO) annotations are marked in the center panel. Locations of binding sites relative to the transcription start site of each gene are represented at right. (**B**) Detailed D-SPOP subnetwork depicting that D-SPOP is regulated by FTZ and EVE and interacts with puc. (**C**) RNA *in situ* hybridization of D-SPOP in wild type and *ftz* mutant backgrounds. 14 and 7 stripes of expression were observed in wild type and *ftz* embryos, respectively. (**D**) D-SPOP and EVE antibody staining in wild type and *eve* mutant backgrounds. D-SPOP (BCIP/NBT, blue) was stained in segmental grooves in wild type but all expression was lost in *eve* mutant embryos. Eve (Diaminobenzidine, brown) was stained in neurons.
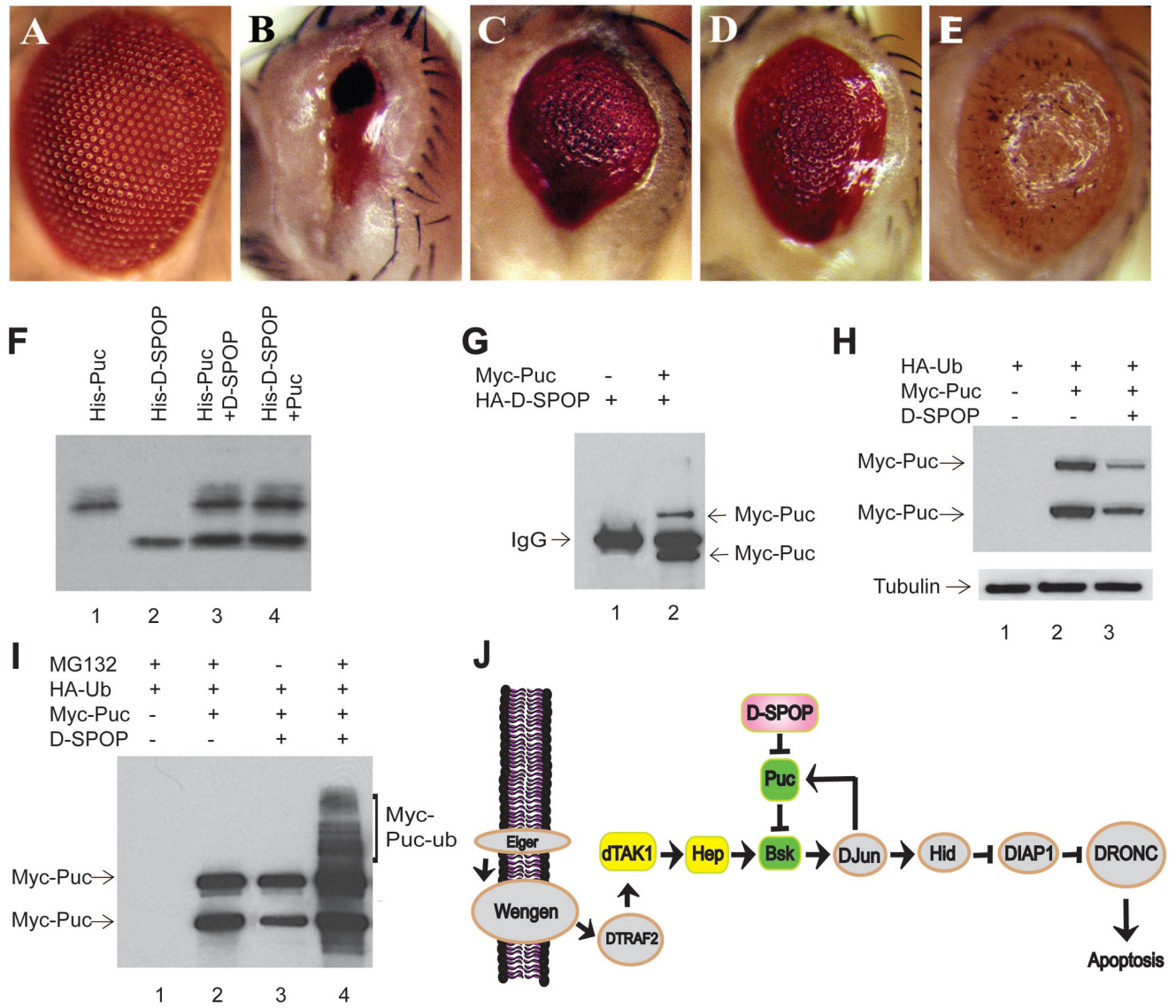
Fig. 2.
D-SPOP promotes puc ubiquitination and degradation. (**A**) Light micrographs of *Drosophila* adult eyes for wild type (GMR-Gal4/+). (**B**) GMR>Egr triggered cell death and produced a small eye phenotype (GMR-Gal4 UAS-Egr/+). (**C**) Deleting one copy of D-SPOP (GMR-Gal4 UAS-Egr/+; D-SPOPΔ6/+) suppressed the phenotype of (GMR-Gal4 UAS-Egr/+). (**D**) Co-expression of D-SPOP RNAi (GMR-Gal4 UAS-Egr/+; UAS-D-SPOP-RNAi) suppressed the phenotype of (GMR-Gal4 UAS-Egr/+). (**E**) Expression of D-SPOP (*GMR*-Gal4 *UAS*-D-SPOP/+) produced rough eyes with slightly reduced size. (**F**) D-SPOP interacts with Puc in an *in vitro* affinity assay. Proteins were translated *in vitro,* purified on a nickel ion (Ni^{++}) column and detected by Western blot (see supplementary methods). Lane 1, His-Puc; Lane 2, His-D-SPOP; Lane 3, untagged D-SPOP co-purifies with His-Puc; Lane 4, untagged Puc co-purifies with His-D-SPOP. (**G**) D-SPOP interacts with Puc in an *in vivo* immunoprecipitation (IP) assay. IPs were carried out with anti-HA antibody using cell lysates from S2 cells expressing the indicated fusion proteins, followed by immunoblot with anti-Myc epitope antibody. Lane 1, IP of HA-D-SPOP control transfection shows only the IgG band; Lane 2, IP of HA-D-SPOP

in cells co-transfected with Myc-Puc, which is detected as two bands. (**H**) Puc degradation is promoted by SPOP. Western blots were performed with anti-Myc antibody to detect Myc-Puc fusion protein. Lane 1, HA-Ubiquitin (HA-Ub) transfection negative control; Lane 2, Myc-Puc transfection positive control; Lane 3, Myc-Puc and D-SPOP co-transfection shows reduction of Myc-Puc levels relative to. Tubulin is detected as a loading control. (**I**) *In vivo* ubiquitination of Puc is promoted by D-SPOP. Myc-Puc was detected by immunoblot with anti-Myc epitope antibody. Lane 1, HA-Ub expression and MG132 treatment as a negative control; Lane 2, HA-Ub and Myc-Puc co-expression with MG132 treatment but without D-SPOP; Lane 3, Myc-Puc levels decreased with co-expression of HA-Ub and D-SPOP but without addition of MG132; Lane 4, Myc-Puc poly-ubiquitination in the presence of HA-Ub, D-SPOP and MG132. (**J**) TNF/Eiger induced apoptosis pathway. D-SPOP (pink) is downstream of dTAK1 (JNKKK, yellow) and Hep (JNKK, yellow), and upstream of Bsk (DJNK, green) and Puckered (MKP, green).

A
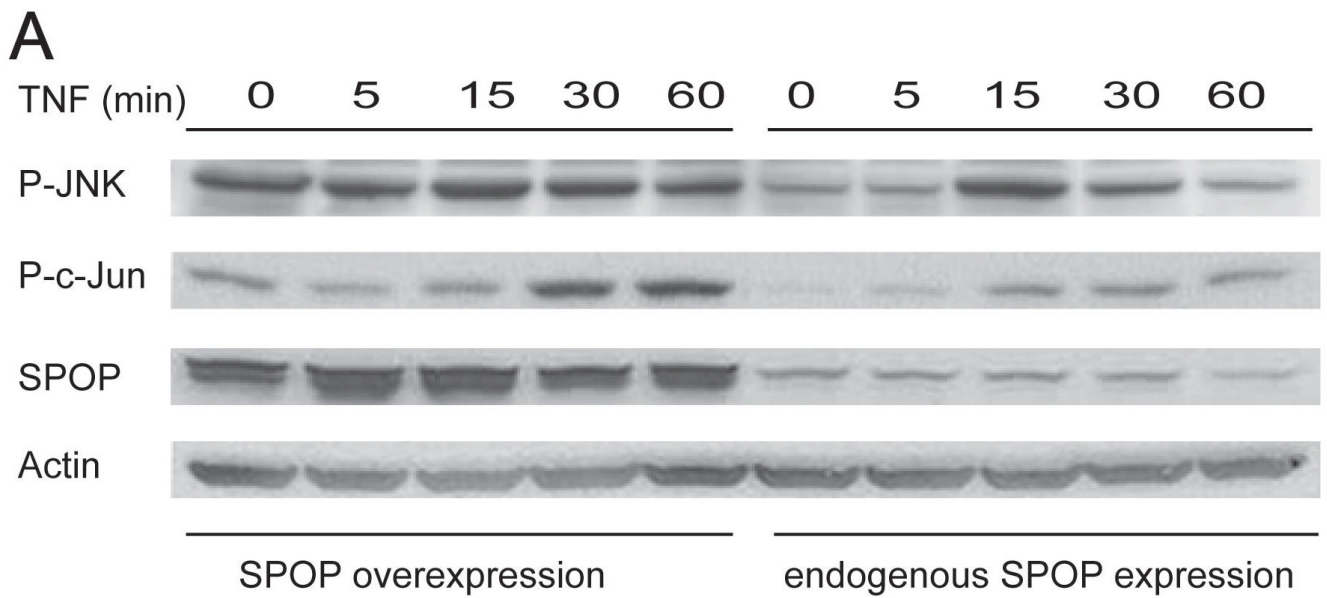
B
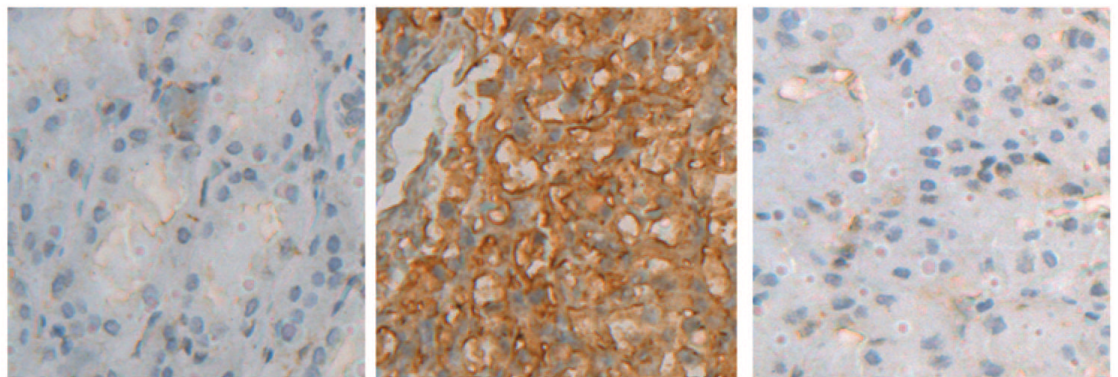
normal   clear   oncocytoma

Fig. 3.
Function of SPOP in the mammalian TNF pathway and over-expression in renal cell carcinoma.
(**A**) Over-expression of SPOP increases the level of P-JNK and P-c-Jun. Human embryonic
kidney (HEK293) cells were transfected with SPOP, treated with 50ng/ml TNF at 0, 5, 15, 30,
60 minutes, followed by immunoblot. In control treatments, HEK293 cells were transfected
with empty pcDNA3.1 vector, and thus only express endogenous levels of SPOP. (**B**) SPOP
expression in RCC tissue. Tissue images are from normal kidney, oncocytoma and clear cell
renal carcinoma. A SPOP-specific monoclonal antibody (SPOP-5G) was used to detect SPOP
expression in tissue (Diaminobenzidine, brown staining).

Table 1

Tissue micro-array screening for SPOP expression in 18 cancer types from different organs.

Tissue Type	Normal Tissue	Cancer Tissue
Kidney/Renal	5 negative	17 positive; 3 negative
Uterus/Endometrial	5 negative	10 positive; 4 negative
Testis/Germ cell	5 weak	18 positive; 2 negative
Soft tissue/Sarcoma	5 negative	20 weak or negative
Lung	5 weak	20 weak
Bladder	5 weak or negative	20 weak or negative
Breast	5 weak or negative	20 weak or negative
Prostate	5 negative	1 positive; 19 negative
Pancreas	5 negative	20 negative
Lymphoma	5 negative	19 weak or negative
Thyroid	5 negative	20 weak or negative
Colon	5 negative	20 negative
Ovary	5 weak or negative	20 weak or negative
Skin/Melanoma	5 weak or negative	20 weak or negative
Liver	5 positive	7 positive; 13 negative
Skin/squamous	5 weak or negative	20 weak or negative
Brain	5 weak or negative	20 weak or negative
Stomach/Gastric	5 weak or negative	20 weak or negative

SPOP is highly expressed in renal cell carcinoma as compared to normal renal tissue. Endometrial carcinoma and germ cell tumors also display higher SPOP staining relative to comparable normal tissues.

Table 2

SPOP expression in RCCs. RCC tissue sections were analyzed by staining with SPOP specific monoclonal antibody (SPOP-5G). Patient samples are classified into different categories depending on cell type.

Renal cell type	positive	negative
clear cell	179	1
chromophobe	6	1
papillary	6	21
oncocytic	2[*]	28
rare type	6	8
Total tumor	199	59
Normal tissue	0	295

[*] Both cases are weak staining.

Table 3

SPOP expression in metastatic lesions where RCC were the primary tumors. Metastatic tissues were analyzed by staining with SPOP specific monoclonal antibody (SPOP-5G). Patient samples are classified into different categories depending on cell type of the primary tumor.

Primary RCC type	positive	negative
clear cell	71	2
chromophobe	3	1
papillary	1	2
rare type	3	4